CWE-8
June 7-11, 2026
London, ON, Canada

Impact of Stoss Slope on Airflow Dynamics over Transverse Dunes in Deserts: Experimental and Numerical Investigations

Sumaja Kolli [a], Pradeep Kumar Dammala [b], Hassan Hemida [c]

[a] *Indian Institute of Technology Jodhpur, Jodhpur, Rajasthan, India, kolli.1@iitj.ac.in*
[b] *Indian Institute of Technology Jodhpur, Jodhpur, Rajasthan, India, pkdammala@iitj.ac.in*
[c] *University of Birmingham, Birmingham, United Kingdom, h.hemida@bham.ac.uk*

SUMMARY

Aeolian soil erosion driven by wind interaction stands as a crucial process in shaping sand dunes and ripples. Current study investigates airflow patterns over transverse dunes of varying stoss slopes (10°, 20°, and 32°) through experimental wind-tunnel and computational fluid dynamic (CFD) studies on scaled dune models. Velocity profiles and surface pressure distributions were measured to examine variations in flow acceleration, stagnation, and separation that drive aeolian erosion. CFD results agree well with experiments, capturing velocity trends, pressure variation, and separation behaviour. Wind speed analysis revealed steeper stoss slopes intensify flow deceleration and enlarge the separation zone, while gentler slopes produce smoother acceleration and delayed separation. Surface pressure distributions supported these findings and reflected similar trends with 10° slope experiencing the highest negative pressure near crest. The separation and reattachment zones detailed zone of recirculation characteristics with steeper dune reflecting strong stagnation and separation zones highlighting probable sand deposition zones. Lee side air flow dynamics are also quantified where increase in slope steepness reflected longer recirculation zone.
Keywords: *Sand Dune, Wind Tunnel, Aeolian Erosion, Computational Fluid Dynamics*

1. INTRODUCTION

Windblown sand disrupts infrastructure and agricultural farmlands, causing severe environmental impacts. The extent of aeolian erosion is highly influenced by the morphology of sand dunes and wind flow patterns in the vicinity. Realizing the impact, many researchers since pioneering work of Bagnold (1941) delved into understanding aeolian erosion. Since sand dunes evolve continuously with time, their interaction with wind and surroundings keeps modifying, hence extensive work was done on understanding on influence of windward and leeward slopes on sand transport dynamics (Walker and Nickling, 2003; Parson et al., 2004; Dong et al., 2007, Faria et al., 2011, Kolli et al., 2026 a,b). Stoss slope plays a key role in governing near-surface acceleration, adverse pressure gradients near the crest, and the size of the lee-side recirculation zone. It can therefore alter erosion potential and sediment transport pathways. Despite these advances, the specific role of variable stoss slopes in transverse dune aerodynamics remains insufficiently quantified, particularly under controlled laboratory conditions where dune height and lee slope are held constant. To address this gap, the present study investigates airflow dynamics over scaled transverse dunes with identical height and lee slope but systematically varied stoss slopes (10°-D10, 20°-D20, and 32°-D32). A combination of wind tunnel experiments and Reynolds-averaged Navier Stokes (RANS) based CFD simulations is employed to quantify wind speed variation, surface pressure distribution, and flow separation characteristics that define wind derived erosion dynamics. The validation of CFD data with wind tunnel experimental data provides further insights into the reliability of RANS models in resolving shallow and steep dune slopes. The outcomes contribute to improved understanding of dune–flow interactions, with implications for aeolian erosion prediction, dune migration modeling, and desert infrastructure planning.

2. METHODOLOGY

2.1. Dune Models

Current study examines scaled dune models of varying stoss slopes (10°, 20° and 32°). All dunes share a common lee slope of 32° and a uniform height of 50 mm. The adopted dune model adheres to the similitude principles outlined by White (1996) and discussed in detail in Kolli et al. (2026 a,b). All the models are 3D printed representing old dunes that are immobilized in nature/stationary dunes with the identical lee slope, matching the angle of repose of soil particles of desert areas (Ferreira and Lambert, 2011; Kolli et al., 2023).

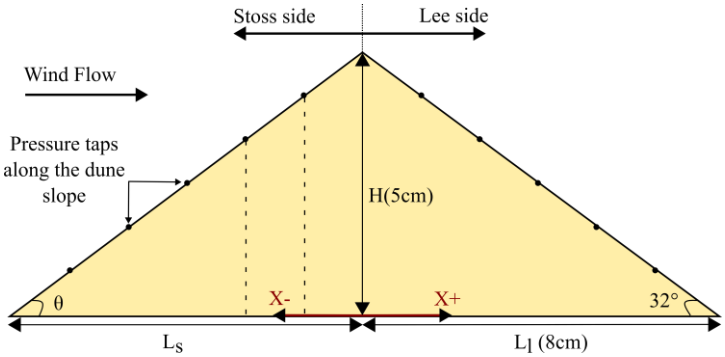

Figure 1 Dune model with varying stoss slope and pressure tap location reference (depicted through X) along base lengths on stoss (L_s) and lee side (L_l)

2.2. Experimental Setup

Experiments were carried out at the subsonic wind tunnel (WT) setup (0.6m x 0.6m x 4m at Indian Institute of Technology Jodhpur, India. The width of models is spanned across the complete width of WT representing a two-dimensional transverse dune. Single channel electronic manometer connected to the pitot static tube is utilized to measure the wind velocities. The streamwise velocity profile at 0.5m from outlet of empty WT matches power law approximation (Eq.(1)) with an exponent (α) of 0.13 similar to the arid settings of White (1996) study on sand dunes, as shown in Figure 2. The power law curve is given by

$$u_z/u_{ref} = (z/z_{ref})^{\alpha} \quad \text{..... (1)}$$

Here u_z and u_{ref} are the streamwise velocities along at height z from the wind tunnel floor and at the reference height, $z_{ref} \approx 0.22$m beyond the boundary layer thickness of 0.18m, respectively. Further, surface pressure distribution across the dune is measured using 8 Port Surface Pressure Scanner system by Sunshine Pvt Ltd. Pressure taps were drilled and attached on the printed dune models. The resultant surface pressure is reported in terms of surface pressure coefficient (C_p), as defined in Eq. (2). While Cp readings were taken along the sloped dune surface, their positions will be reported along the base length of dune (X direction) illustrated in Figure 1.The center of the dune base is taken as the reference point ($X = 0$), with the stoss side defined as negative ($X < 0$) and the lee side as positive ($X > 0$).

$$C_p = \frac{p - p_\infty}{0.5\rho u_{ref}^2} \quad \text{..... (2)}$$

Here p is actual pressure at the surface pressure tap, p_∞ is the free stream (reference) pressure, and ρ represents the density of air.

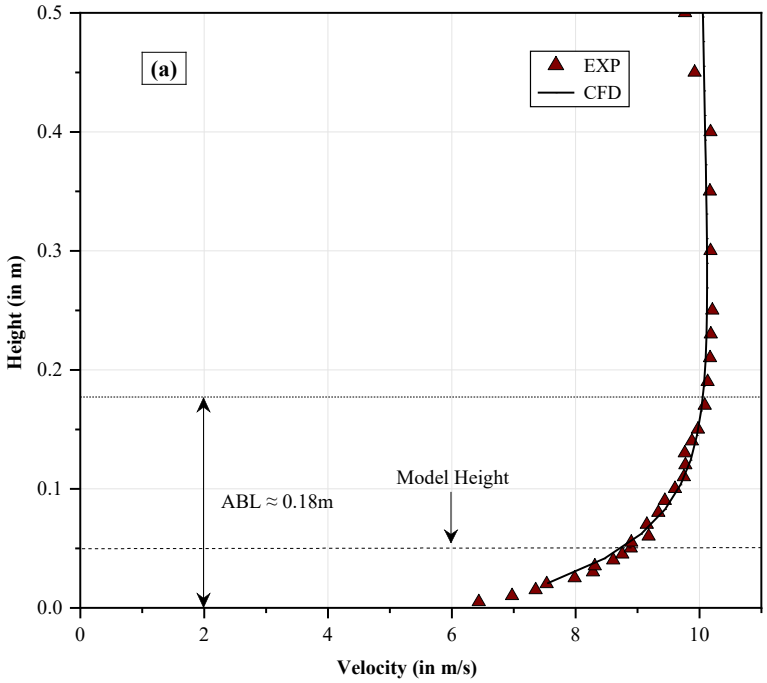

Figure 2 Inlet wind velocity profile from experimental wind tunnel setup (line) and CFD simulations (marker)

2.3. Numerical Setup and Methodology

The current setup employs commercially available Computational Fluid Dynamics (CFD) code CFX (ANSYS, 2024) for numerical modelling. CFX utilizes finite volume discretization method to solve the 3D Reynolds Average Navier's Stokes (RANS) equation. Existing studies focusing on numerical modelling on aeolian sand transport reported reliable outputs based on RANS, validated by experimental wind tunnel investigations (Faria et al., 2011; Tominaga et al., 2018). A fully developed homogeneous turbulent state is planned to be considered where a standard shear stress transport (SST) model is employed to solve the corresponding Reynolds-averaged Navier-Stokes equations of motion. The numerical convergence is set to 10^{-5} for all the normalized residuals.

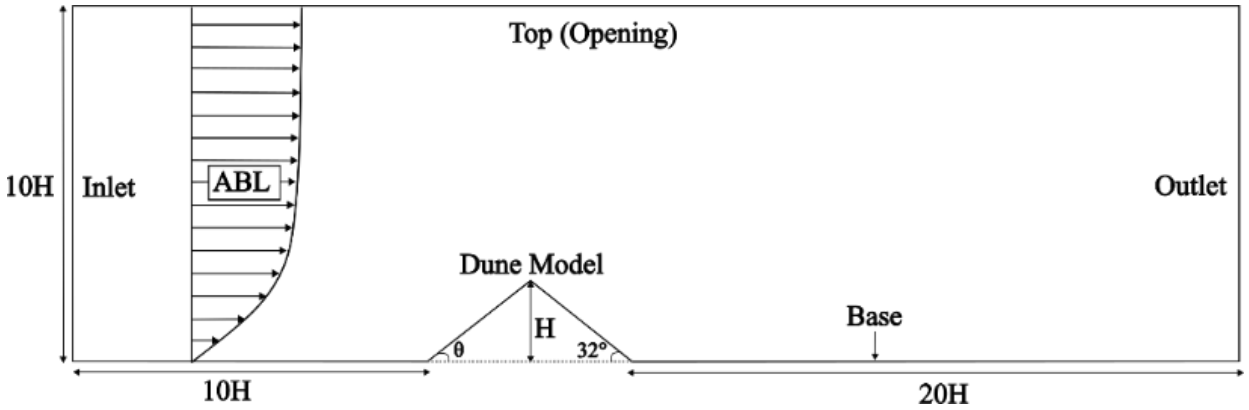

Figure 3 Dimensions of the Computational Domain

The size of the computational domain (refer Figure 3) is defined by the grid independence tests. The inflow in the computational domain is defined at the inlet with the velocity profile matching the wind tunnel inlet velocity profile as shown in Figure 2. The outflow is set to be fully developed

conditioned and zero gradient with zero relative static pressure. The dune model, top and side walls of the computational domain are treated as wall with no slip condition. Further, the obtained results of simulations were validated by comparing the surface pressure readings of wind tunnel experiment with computational results.

3. RESULTS AND DISCUSSION

3.1. Surface Pressure Distribution

Surface pressure coefficient (C_p) distribution on the stoss and lee sides of dune models is depicted in Figure 4. The pressure distributions from numerical CFD simulations are also reported and validated through experimental wind tunnel data in Figure 4(a) and 4(b). A monotonic decrease in Cp is realised in all dune models as the wind flow on stoss ascends towards the dune crest. Lowest Cp values were reported by gentler slope (D10) reflecting its higher and more sustained acceleration along the windward face. In contrast, the steepest dune, D32, exhibits a noticeably milder reduction in C_p, indicating the influence of a stronger adverse pressure gradient that suppresses acceleration and increases flow resistance. These differences become most evident near the crest, where D32 attains the highest (least negative) $C_p$value, signifying weaker suction and a greater likelihood of flow detachment. D20 shows intermediate behavior, closely following the trend between D10 and D32. Numerical predictions capture these patterns well, demonstrating good agreement in both the magnitude and slope-dependent ranking of the pressure distributions. A small deviation is noted for D10, where CFD slightly overpredicts, the pressure drops on the stoss side. This is likely due to the challenges of resolving the thin, gradually accelerating boundary layer over the gentle slope and the tendency of incorporated model to overestimate streamline curvature. Nevertheless, both CFD and experiments exhibit consistent trends, indicating that the discrepancy affects only magnitude and not overall aerodynamic behavior. On the lee side, all dunes display a characteristic plateau in C_p, marking the presence of a separated shear layer and the associated recirculation zone. D32 produces the largest and deepest low-pressure region, followed by D20 and D10, consistent with the stronger separation tendency of steeper dunes.

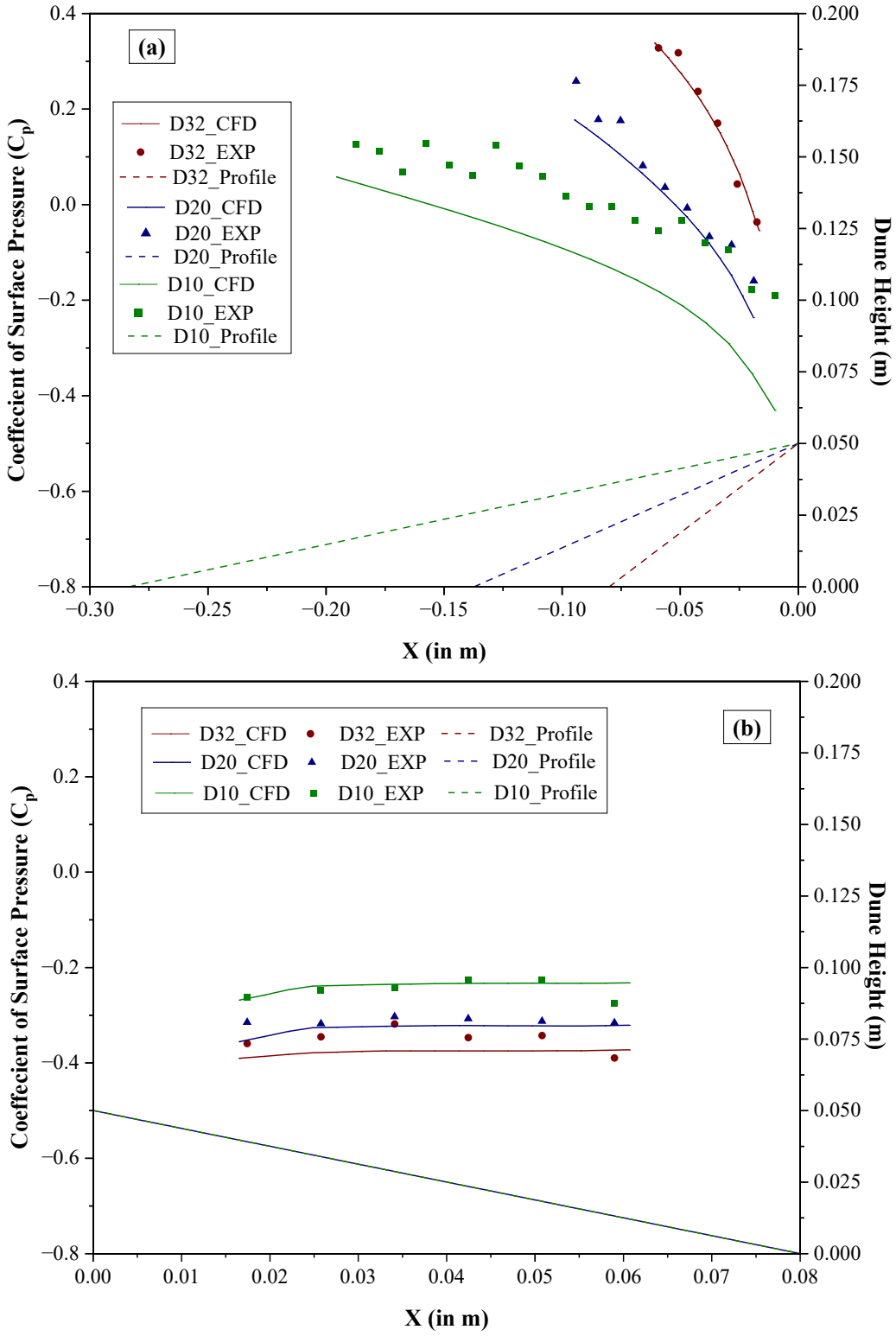

Figure 4 Variation of C_p at centre of dune along the length (a) Stoss side and (b) Lee side

3.2. Airflow Dynamics over dune slope

3.2.1. Wind flow characteristics over stoss side

Windward side of dune (stoss side) experiences streamline compression resulting in flow acceleration towards crest. The initial stagnation upon hitting dune toe is recovered as flow approaches the crest. While this is wide known phenomenon the quantification of flow acceleration and recover from stagnation at dune toe decides the extent of erosion. In current study, the wind speed up ratio as defined in Eq.1 is reported across the stoss slope of dune surface in Figure 5. The wind speed ratio (WSU) is defined as

$$\text{WSU} = u_{1mm}/u_{ref}$$

where u_{1mm} is the wind speed measured 1mm above dune surface along the slope and u_{ref} is the reference wind speed as detailed in Section 2.2.

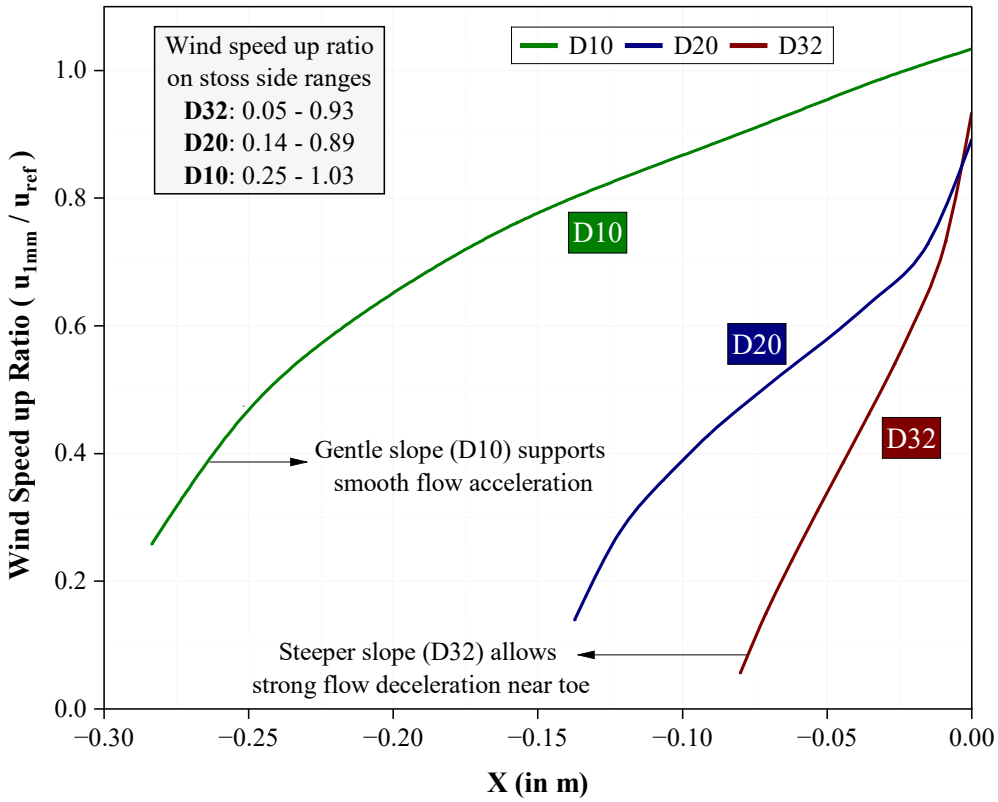

Figure 5. Wind speed up ratio (u_{1mm}/u_{ref}) along the stoss side of dunes. X refers to base length of dunes as shown in Figure 1

A generalized trend of increase in wind speed up ratio is noted as flow approaches towards the crest. Near to the toe of dune, lowest speed-up ratio of 0.05 is exhibited by the steepest slope (D32) highlighting the stagnation effect induced by abrupt steeper slope. In contrast, gentler slopes with rather smoother transition maintain comparatively higher speed-up ratios (D10-0.25 and D20-0.14) at these initial stages. While gentler slopes reported a smooth WSU increase toward the crest ($X \longrightarrow 0$), D32 undergoes a sharper acceleration due to the compressed streamline curvature near the crest. Ultimately, D10 reaches the highest peak speed-up ratio, approaching or slightly exceeding unity, which corresponds to near-crest flow destabilization and the onset of flow

separation immediately downstream. It is also interesting to note that while the jump in WSU ratio from toe to crest is highest for D32 (0.05-0.93), the highest WSU across the stoss side is observed for D10 with WSU range 0.25-1.03.

3.2.2. Wind flow characteristics over lee side

The lee side of dunes is characterized by the zone of recirculation following the separation at the dune crest. While recirculation is observed in all three dune models, the characteristics of recirculation such as the length (L_r) and center (C_r) of recirculation zone, separation and attachment points varied drastically with stoss slope of dunes as detailed in Table 1. Steeper slope with stronger separation at the dune crest resulted in longer length of recirculation in lee side. This pattern highlights the longer trail of sand deposition in lee side of steeper dunes due to the adverse pressure gradient and weak wind induced shear required for transporting the sand particles. Further, as stoss slope tends to be gentler, the length of recirculation zone has reduced to 7H for D10 and 9H for D20. These observations are consistent with Qian et al. (2009) study reporting an L_r of approximately 7.5H and 10.5H for windward slopes of 10° and 20° respectively.

Table 1 Variation of length and center of zone of recirculation for dune models

Model	Length of recirculation zone	Center of recirculation zone
D32	10H (0.5m)	4-4.5H (0.2085m from crest)
D20	9H (0.45m)	3-3.5H (0.159m from crest)
D10	7H (0.35m)	2.5-3H (0.137m from crest)

Further, the trail of separation and reattachment points as shown in Figure 6 define the dune migration patterns. It is realized from Figure 6(a-c) that irrespective of stoss slope variation, dune crest exhibits a consistent separation line that leads to zone of recirculation as detailed in Table 1. However, the stoss side of dune varied drastically in steeper slope (D32) with stagnation zone at toe, inducing a separation line ahead of dune toe followed by reattachment point on stoss slope near to toe (see Figure 6a). While D20 also exhibited similar separation line near toe, it is nearer to the toe than D32 with reattachment points almost exactly at the dune toe. The interesting observation lies in D10 where no separation or reattachment lines were observed due to the gentler stoss slope of dune model resulting in almost no stagnation and minimal disturbance near dune toe (refer Figure 6c). Apart from the dynamics at dune toe, the separation lines are noted to be observed only at the centre line in D32 but tend to be distributed for D20 and D10. The distribution of separation lines on stoss side link as well as lee side link with migration patterns observed in Kolli et al., (2026a). The migration patterns followed ripple formations or disturbances consistent with separation lines. Current study is in process of establishing vortex formation in lee side to deepen the understanding of aeolian dune aerodynamics as detailed in Future work section.

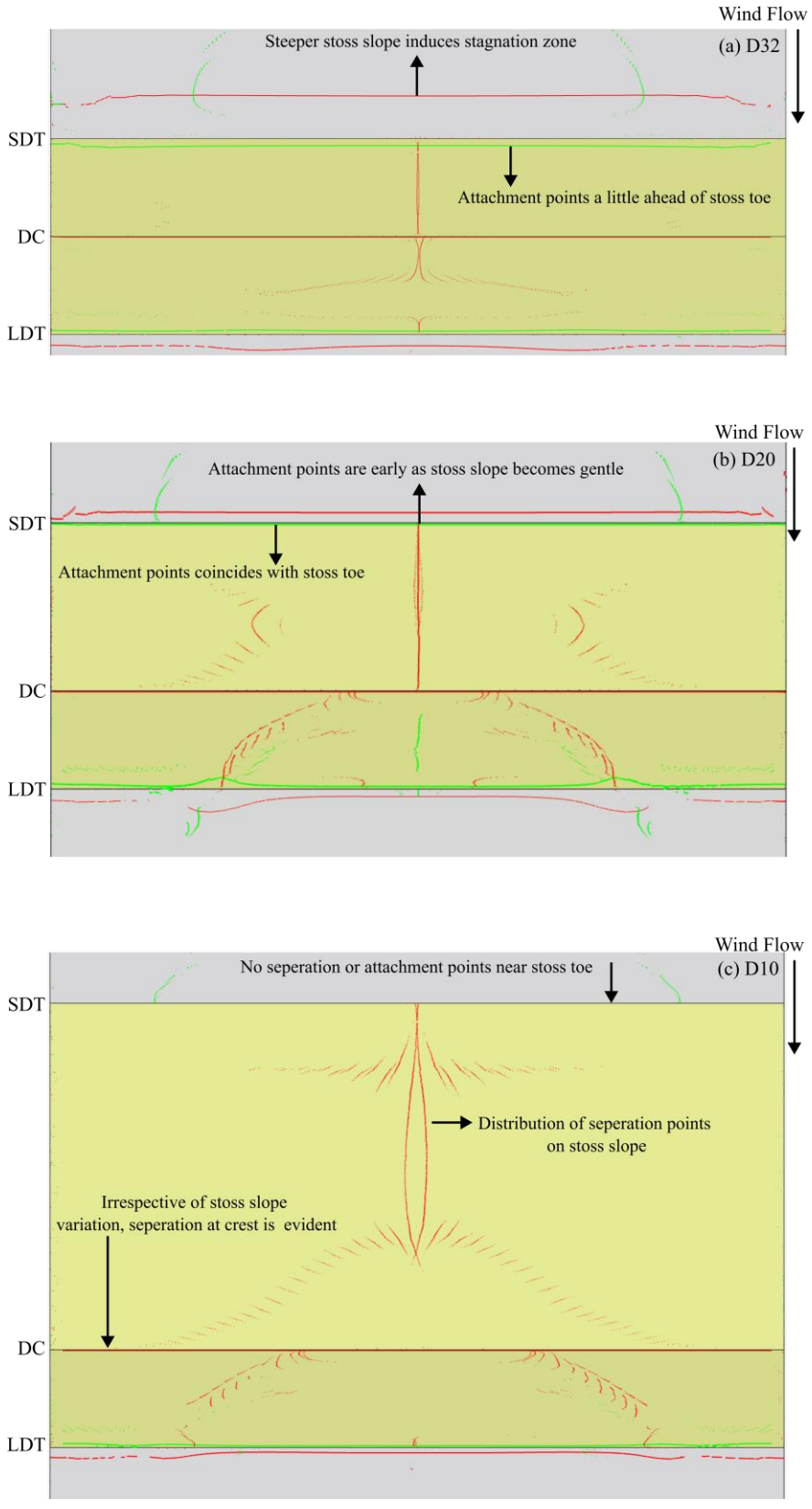

Figure 6. Distribution of flow separation (red) and reattachment (green) lines on dune slope. Here SDT, DC and LDT represent Stoss Dune Toe, Dune Crest and Lee Dune Toe of dune models -D32(a), D20(b) and D10(c).

4. CONCLUSIONS

Current study presents an experimental wind tunnel and numerical CFD studies on scaled dunes of varying stoss slope and constant lee slope to detail the aerodynamic influence in aeolian erosion of sand dunes. Wind speed-up ratio reflected gentler slopes (D10, D20) promote smoother acceleration along the stoss surface, while the steepest slope (D32) induces initial stagnation followed by rapid near-crest acceleration leading to erosion. Stoss-side pressure distributions mirror these trends, with D10 producing the most negative pressures and D32 experiencing a milder drop due to enhanced adverse pressure gradients. On the lee side, all models display a distinct low-pressure plateau associated with flow separation, with the depth and reattachment length increasing systematically with stoss-slope steepness. Lee side characterized by recirculation zones hosts the sand grains eroded from stoss side and depositing in here. Further, numerical results show strong agreement with experimental trends for both stoss and lee sides, reliably capturing velocity profile, surface pressure distribution, separation behavior, and reattachment locations. This consistency indicates that the RANS-based numerical approach, when supported by an appropriate boundary-layer inflow specification, can reliably reproduce key aerodynamic features over dune geometries. Although the current investigation focuses on stationary dunes under unidirectional flow, future studies could incorporate mobile dune configurations and multidirectional wind conditions to further advance understanding of dune-flow interactions.

ACKNOWLEDGEMENTS

We thank the Commonwealth Scholarship Commission in the UK (CSC) for funding the academic visiting period at University of Birmingham, UK.

REFERENCES

Bagnold, R. A. 1941. The physics of blown sand and desert dunes. Boca Raton, FL: Chapman & Hall.

Parsons, D. R., Walker, I. J., & Wiggs, G. F. (2004). Numerical modelling of flow structures over idealized transverse aeolian dunes of varying geometry. Geomorphology, 59(1-4), 149-164.

Walker, I. J., & Nickling, W. G. (2003). Simulation and measurement of surface shear stress over isolated and closely spaced transverse dunes in a wind tunnel. Earth Surface Processes and Landforms: The Journal of the British Geomorphological Research Group, 28(10), 1111-1124.

Dong, Z., Qian, G., Luo, W., & Wang, H. (2007). A wind tunnel simulation of the effects of stoss slope on the lee airflow pattern over a two-dimensional transverse dune. Journal of Geophysical Research: Earth Surface, 112(F3).

Faria, R., Ferreira, A. D., Sismeiro, J. L., Mendes, J. C., & Sousa, A. C. (2011). Wind tunnel and computational study of the stoss slope effect on the aeolian erosion of transverse sand dunes. Aeolian Research, 3(3), 303-314.

Kolli, S., Bind, A., Dammala, P. K., & Hemida, H. (2026a). Influence of sand dune geometry on aeolian erosion and dune migration: a wind tunnel study. *Wind and Structures*, *42*(2), 197.

Kolli, S., Hemida, H., & Dammala, P. K. (2026b). Understanding aeolian processes across sand dunes with varying stoss slope: Wind tunnel experiments. *Geomorphology*, 110177.

White, B. R. (1996). Laboratory simulation of aeolian sand transport and physical modeling of flow around dunes. Annals of Arid Zone, 35(3).

Dammala, P. K., Kolli, S., Garaga, R., Reddy, K. R., & Kumar, P. (2025). Aeolian sand dune fixation–critical review of measures, challenges and future perspectives with a case study on Thar Desert. CATENA , 250 , 108786.

Kolli, S., Dammala, P. K., Ul Haq, A., & Reddy, K. R. (2023). Valorization of Scrapped Marble Slurry Powder as Potential Sand Dune Stabilizer: Pilot Studies on Thar Desert Soils. Journal of Hazardous, Toxic, and Radioactive Waste, 27(4), 04023025.

Tominaga, Y., Okaze, T., & Mochida, A. (2018). Wind tunnel experiment and CFD analysis of sand erosion/deposition due to wind around an obstacle. Journal of Wind Engineering and Industrial Aerodynamics, 182, 262-271.